BEAM AND FINITE ELEMENT MODELS FOR FIBER-BRIDGING IN UNIDIRECTIONAL DCB SPECIMENS

András Szekrényes

Ph.D. Student
Department of Applied Mechanics, Budapest University of Technology and Economics
H-1521 Budapest, Hungary, Phone: +36 1 463 1170, E-mail: szeki@mm.bme.hu

ABSTRACT

This study presents models, based on simple beam theory and the Winkler foundation analysis through the DCB test method. The main goal of this study is to characterize the fiber-bridging phenomen. The bridging fibers were modeled by tensile beams. Finite element models were also constructed, the bridging fibers were represented by TRUSS2D elements, the strain energy release rate was evaluated using the J-integral and the VCCT technique. The results of the models were compared with experimental ones taken from literature. It can be concluded that the bridging fibers are necessary to be considered to eliminate the overpredictions in the mode-I fracture toughness.

1. INTRODUCTION

The standard DCB method is suitable to measure the mode-I interlaminar fracture toughness of laminated composite materials. The arms of the DCB specimen can be modeled as homogeneous beams. In literature several authors occupy with the construction of more sophisticated models (advanced beam models). Olsson summarized these models, including the Saint-Venant effects, transverse shear, and crack-tip rotation using the Winkler foundation model [1]. Ozdil and Carlsson also used the Winkler model for unidirectional and angle-ply DCB specimens [2]. However these models can provide the desired accuracy, no theoretical and FE models were constructed which account for the fiber-bridging phenomen until now.

2. BEAM ANALYSIS OF THE DCB SPECIMEN

Considering the DCB specimen in Fig.1.a including one bridging the deflection function is governed by the differential equation shown below:

$$\frac{d^2 w(x)}{dx^2} = \frac{-M_b(x)}{I_y E_x}, \quad -a \le x \le 0.$$ (1)

The DCB specimen in Fig.1.b, including the Winkler foundation in the uncracked region ($w_{l3}(x)$, $w_{u3}(x)$) is governed by the following equation (Eq.1 is still valid) :
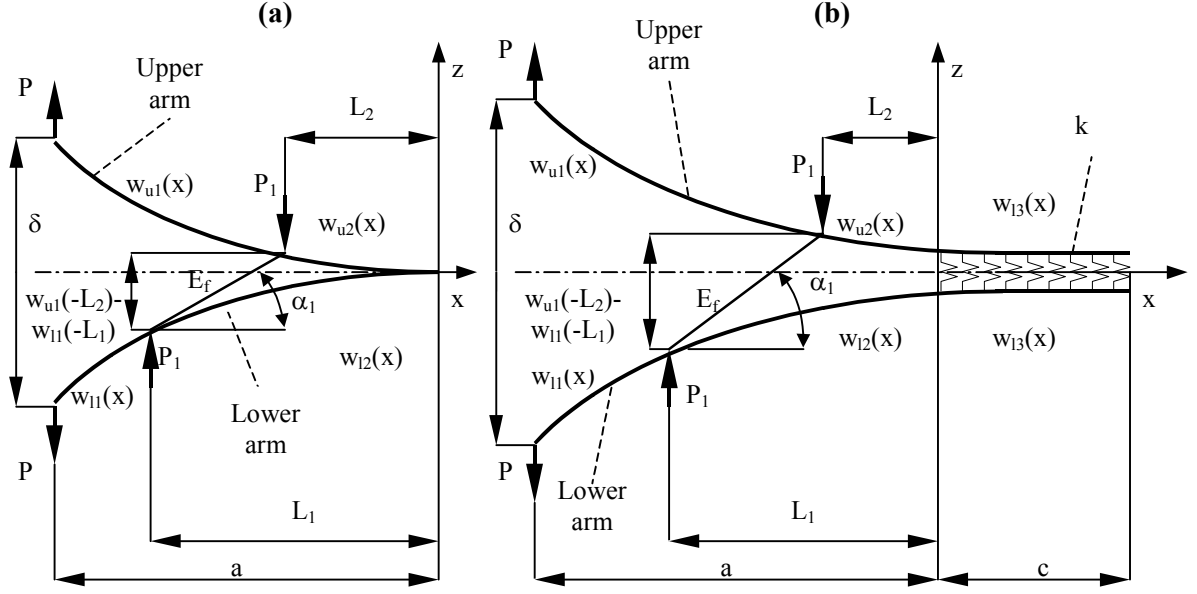
Fig.1.

Two formulation of the fiber-bridging phenomen. Model based on simple beam theory (a), model based on the Winkler foundation analysis (b).

$$\frac{d^4 w(x)}{dx^4} + 4\lambda^4 w(x) = 0 \ , \qquad \lambda = \frac{6^{1/4}}{h}\left(\frac{E_z}{E_x}\right)^{1/4} , \qquad 0 \le x \le c . \tag{2}$$

For the lower arm of the specimen in the delaminated region the deflection functions can be expressed as follows:

$$w_{l1}(x) = -\frac{P\left(\frac{1}{2}ax^2 + \frac{1}{6}x^3\right)}{I_y E_x} + c_1 x + c_2 , \quad -a \le x \le -L1 , \tag{3}$$

$$w_{l2}(x) = -\frac{P\left(\frac{1}{2}ax^2 + \frac{1}{6}x^3\right) + P_1\left(\frac{1}{2}L_1 x^2 + \frac{1}{6}x^3\right)}{I_y E_x} + c_3 x + c_4 , \quad -L1 \le x \le 0 . \tag{4}$$

In the uncracked region (Fig.1.b) Eq.2 can be solved by combining the homogeneous generalized Krulov-functions $(V_1(x), \ V_2(x), \ V_3(x), V_4(x))$, which can be found elsewhere, hence he deflection in the uncracked region:

$$w_{l3}(x) = c5 \cdot V_1(x) + c6 \cdot V_2(x) + c7 \cdot V_3(x) + c8 \cdot V_4(x) , \qquad 0 \le x \le c . \tag{5}$$

It was assumed that the bridging fiber is connected to the arms with pins. According to this the elongation in the bridging fiber:

$$\Delta r_1 = \sqrt{[w_{u1}(x = -L_2) - w_{l1}(x = -L_1)]^2 + L_{01}^2} - L_{01} , \tag{6}$$

where $L_{01} = L_1 - L_2$ is the initial length of the bridging. The tensile force in the bridging:

$$F_1 = s_1 \Delta r_1, \qquad s_1 = \frac{A_1 E_f}{L_{01}}, \tag{7}$$

where s_1 is the stiffness, A_1 is the cross-section of the bridging bundle. The next step is to express the off-axis angle between the fiber and the x-axis:

$$\alpha_1 = \arctan\left(\frac{w_{u1}(x=-L_2) - w_{l1}(x=-L_1)}{L_2 - L_1} \right). \tag{8}$$

Hence the force P_1 which loads the DCB specimen, according to Fig.:

$$P_1 = F_1 \sin\alpha_1. \tag{9}$$

The deflection functions can be expressed using the proper boundary and matcing conditions, for the model in Fig.1.a: $w_{l1}(0)=w'_{l1}(0)=0$, for the model in Fig.1.b: $w_{l2}(0)=w_{l3}(0)$, $w'_{l2}(0)=w'_{l3}(0)$, $w''_{l3}(c)=w'''_{l3}(c)$ and for both models: $w_{l1}(-L_1)=w_{l2}(-L_1)$, $w'_{l1}(-L_1)=w'_{l2}(-L_1)$, and similarly also for the upper arms. Substituting Eq.6, Eq.7 and Eq.8 into the expression of P_1 (Eq.9) and substituting the displacements $w_{l1}(x=-L_1)$ and $w_{u1}(x=-L_2)$ into the formula of α_1 in Eq.8 yields a transcendent equation, which can be solved for P_1 by a numerical procedure. In fact in the case of fiber-bridging several debonded fiber bundles can be observed as reported and photographed by several authors [3,4]. The procedure can be generalized for 'i' number of bridgings. In this case an equation system is resulted, which should be solved numerically for the disinct P_i forces. After the equation system has been solved for the forces, the compliance $(C=\delta/P)$ of the DCB specimen can be obtained by expressing and subtracting $w_{l1}(x=-a)$ from $w_{u1}(x=-a)$ and dividing by force P. The compliance of the specimen based on simple the model in Fig.1.a:

$$C = \frac{8a^3}{E_x bh^3} - \sum_{i}^{n} \frac{\beta \cdot 2P_i}{P} \left(\frac{3a(L_{2i-1}^2 + L_{2i}^2) - (L_{2i-1}^3 + L_{2i}^3)}{E_x bh^3} \right). \tag{10}$$

The fracture toughness can be obtained by using the Irwin-Kies expression:

$$G_I = \frac{P^2}{2b} \frac{dC}{da}, \tag{11}$$

hence the fracture toughness:

$$G_I = \frac{12P^2 a^2}{E_x bh^3} - \sum_{i=1}^{n} \frac{3\beta \cdot PP_i(L_{2i-1}^2 + L_{2i}^2)}{E_x bh^3}. \tag{12}$$

Considering the model in Fig.1.b and assuming that the length of the uncracked region (c) is much larger than the specimen thickness (h), after some simplifications the following equations can be derived for the compliance:

$$C_{DCB} = C_{DCB}^0 - \sum_{i=1}^{n} \frac{2\beta \cdot P_i}{PE_x bh^3} \left(\begin{array}{l} 3a(L_{2i-1}^2 + L_{2i}^2) - (L_{2i-1}^3 + L_{2i}^3) + 3.83ah(L_{2i-1} + L_{2i})\left(\frac{E_x}{E_z}\right)^{\frac{1}{4}} \\ + 1.22h^2(L_{2i-1} + L_{2i} + 2a)\left(\frac{E_x}{E_z}\right)^{\frac{1}{2}} + 1.56h^3\left(\frac{E_x}{E_z}\right)^{\frac{3}{4}} \end{array} \right), (13)$$

$$C_{DCB}^0 = \frac{8a^3}{E_x bh^3}\left(1 + 1.92\left(\frac{h}{a}\right)\left(\frac{E_x}{E}\right)^{\frac{1}{4}} + 1.22\left(\frac{h}{a}\right)^2\left(\frac{E_x}{E_z}\right)^{\frac{1}{2}} + 0.39\left(\frac{h}{a}\right)^3\left(\frac{E_x}{E_z}\right)^{\frac{3}{4}}\right), \quad (14)$$

where the term C_{DCB}^0 is the specimen compliance based on the Winkler foundation model, which was referred by Olsson [1]. The term C_{DCB}^{FB} accounts for fiber-bridging in the delaminated region. Based on the current beam analysis the fracture toughness can be obtained by differentiation using Eq.(11):

$$G = G_I^0 - \sum_{i=1}^{n} \frac{\beta \cdot PP_1}{E_x b^2 h^3}\left(3(L_{2i-1}^2 + L_{2i}^2) + 3.83h(L_{2i-1} + L_{2i})\left(\frac{E_x}{E_z}\right)^{\frac{1}{4}} + 2.45h^2\left(\frac{E_x}{E_z}\right)^{\frac{1}{2}}\right), (15)$$

$$G_I^0 = \frac{12Pa^3}{E_x b^2 h^3}\left(1 + 1.28\left(\frac{h}{a}\right)\left(\frac{E_x}{E}\right)^{\frac{1}{4}} + 0.41\left(\frac{h}{a}\right)^2\left(\frac{E_x}{E_z}\right)^{\frac{1}{2}}\right). \tag{16}$$

Again the term G_I^0 is derived by Olsson, the term G_I^{FB} exists if fiber-bridging is observable in the cracked region. In Eq.13 and Eq.15 $\beta=2$ for symmetric, $\beta=1$ for asymmetric arrangements of the bridging fibers, and n is the number of distinct forces due to fiber-bridging.

3. FINITE ELEMENT MODELS

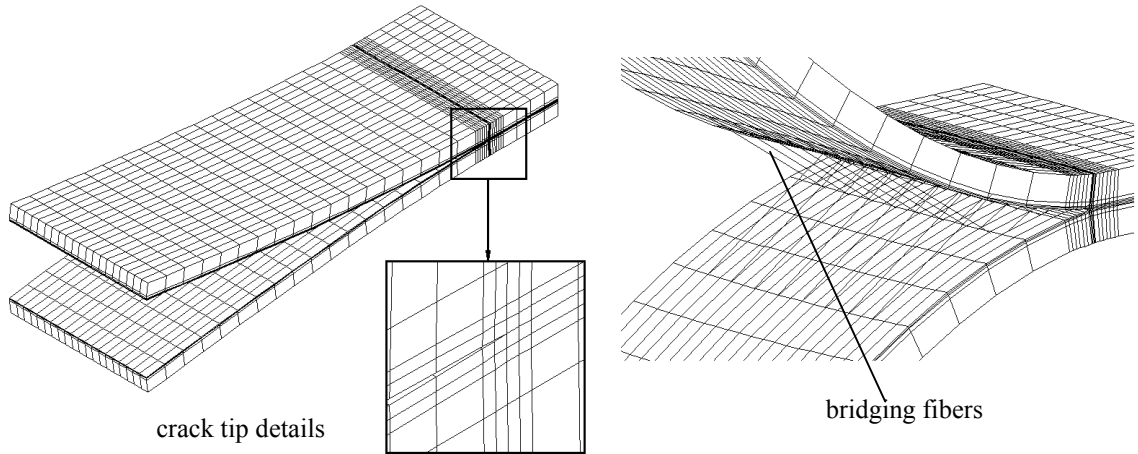crack tip details

bridging fibers

Fig.2.
3D finite element model, including crack-tip details and bridgings

In the current study two and three-dimensional FE models were constructed using the commercial finite element code COSMOS/M 2.0. The 2D model utilizes PLANE2D elements in plain strain, while in the 3D analysis eight-noded, layered composite SOLIDL elements were used. The strain energy release rate was calculated using the J-integral in the 2D and the virtual crack closure technique (VCCT) in the 3D model. The bridging fibers were represented by TRUSS2D elements. The 3D models were used to investigate the effect of fiber-bridging on the strain energy distribution along the crack front. The 3D finite element model is illustrated in Fig.2 including the crack tip details and the fiber-bridgings, the 2D model is very similar.

4. RESULTS AND DISCUSSION

The compliance and fracture toughness obtained from the models was compared with the experiments presented by Morais et al. [5]. Load-displacement data was used as input in the models. Considering the compliance curves in Fig.3 it can be
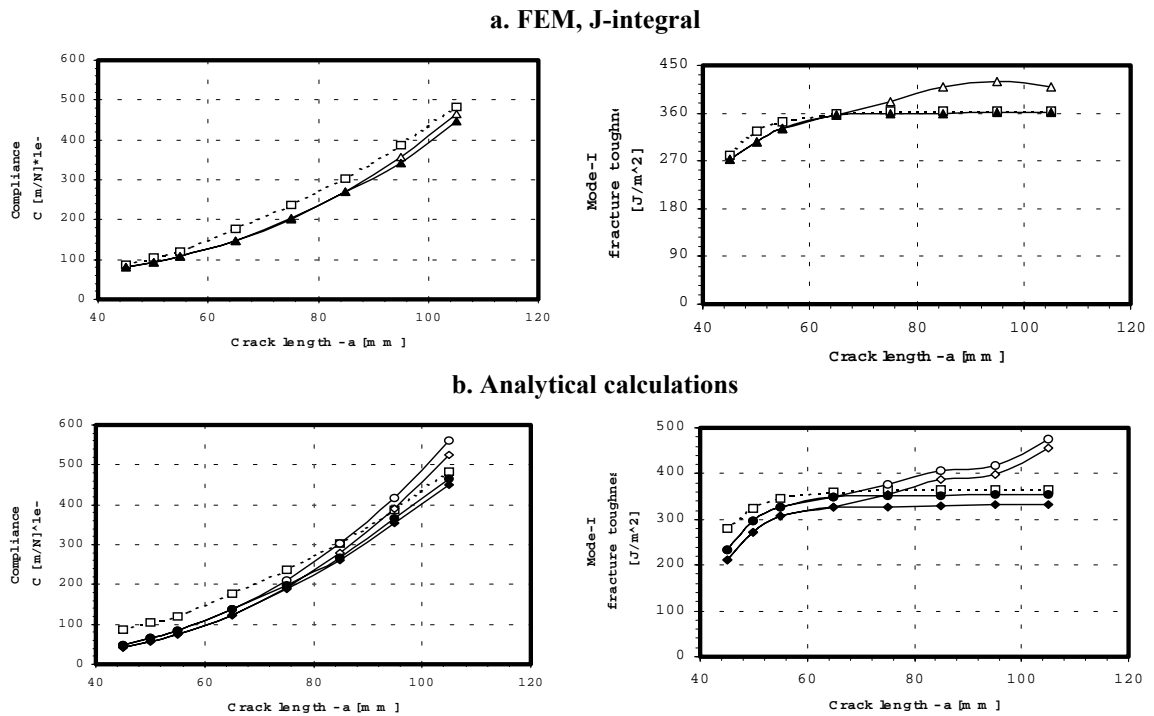
a. FEM, J-integral

b. Analytical calculations

Fig.3.
Compliance and R-curves for the carbon/epoxy DCB specimens.
Experiments according to Morais et al. [□], 2D FE model without [Δ] and with fiber-bridgings [▲], simple beam model without [◊] and with fiber-bridgings [♦] (Eq.10 and 12), Winkler model without [O] (Eq.14 and 16) and with fiber-bridgings [●] (Eq.13 and 15).

seen that the experimental values are slightly lower than the values from the FE and model predictions. The models including fiber-bridging gives closer values in comparison with the models without them, however there is not any significant difference in the two analytically obtained curves. The difference in the fracture toughness can be seen in the R-curves of the FE analysis. In Fig.3 the J-integral significantly overestimates the fracture toughness in the final stage of the delamination process if the assumed bridging fibers are missing. Since the J-integral gives

reasonably good results until the crack length of a=65 mm it was assumed, that the fiber-bridging is the main cause of the former overpredictions. The corrected values are also depicted in Fig.3. In all the specimens it was estimated that the bridging bundles consist of 50-100 single fibers. The fiber-bridging form used was symmetrical arrangements and the number of bridging pairs was increased until 4-5 pieces until the final crack length. Considering the results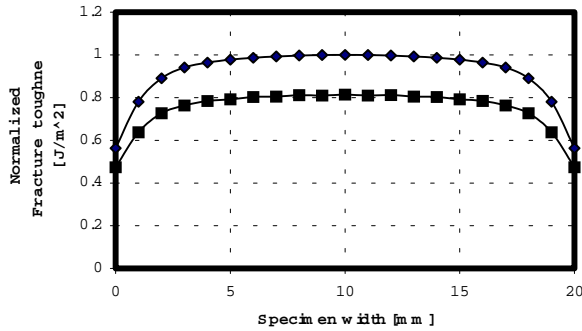 of the simple beam theory without fiber-bridging no steady-state toughness can be determined. The beam theory with bridging bundles partially eliminates this effect. The best results were obtained in the case, including fiber-bridging and the elastic foundation. The effect of the fiber-bridging on the distribution of the fracture toughness along the specimen width is depicted in Fig.4. The bridgings (symmetric arrangements were applied) decrease the width-wise average and also eliminates the overpredictions. The fracture energy was normalized by the width-wise maximum.

Fig.4 The effect of fiber-bridging in the distribution of the fracture toughness, without fiber-bridging [♦], including bridging fibers [■]

5. CONCLUSIONS

The fiber-bridging phenomen in unidirectional carbon/epoxy DCB specimens was analysed based on simple beam theory, the Winkler foundation model and the finite element method. Results show, the bridging fibers are necessary to be considered for accurate predictions of the specimen compliance and the mode-I fracture toughness in comparison with experiments. The fracture toughness was predicted fully analitically and very good predictions were made based on the current models.

6. REFERENCES

[1]   OLSSON R.: **A simplified improved beam analysis of the DCB specimen**. Composites Science and Technology, 1992;43;329-338

[2]   OZDIL F., CARLSSON L.A.: **Beam analysis of angle-ply laminate DCB specimens**. Composites Science and Technology, 1999;59;305-315

[3]   TANZAWA Y., WATANABE N., ISHIKAWA T.: **FEM simulation of a modified DCB test for 3-D orthogonal interlocked fabric composites**. Composites Science and Technology, 2001;61;1097-1107

[4]   HASHEMI S., KINLOCH J., WILLIAMS J.G. **Mechanics and mechanisms of delamination in a poly(ether sulphone)-fibre composites**. Composites Science and Technology, 1989;378;429-462

[5]   MORAIS A.B., MOURA M.F., de, MARQUES A.T., CASTRO P.T.: **Mode-I interlaminar fracture of carbon/epoxy cross-ply laminates**. Composites Science and Technology, 2002;62;679-686